

# Effects of Hyperfine Particles on Reflectance Spectra from 0.3 to 25 $\mu\text{m}$

JOHN F. MUSTARD AND JOHN E. HAYS

*Department of Geological Sciences, Brown University, Providence, Rhode Island, 02912*  
E-mail: mustard@porter.geo.brown.edu

Received November 30, 1995; revised July 5, 1996

Fine grained particles  $<50 \mu\text{m}$  in size dominate particle size distributions of many planetary surfaces. Despite the predominance of fine particles in planetary regoliths, there have been few investigations of the systematic effects of the finest particles on reflectance spectra, and on the ability of quantitative models to extract compositional and/or textural information from remote observations. The effects of fine particles that are approximately the same size as the wavelength of light on reflectance spectra were investigated using narrow particle size separates of the minerals olivine and quartz across the wavelength range 0.3 to 25  $\mu\text{m}$ . The minerals were ground with a mortar and pestle and sieved into five particle size separates of 5- $\mu\text{m}$  intervals from  $<5 \mu\text{m}$  to 20–25  $\mu\text{m}$ . The exact particle size distributions were determined with a particle size analyzer and are shown to be Gaussian about a mean within the range of each sieve separate. The reflectance spectra, obtained using a combination of a bidirectional reflectance spectrometer and an FTIR, exhibited a number of systematic changes as the particle size decreased to become approximately the same size and smaller than the wavelength. In the region of volume scattering, the spectra exhibited a sharp drop in reflectance with the finest particle size separates. Christiansen features became saturated when the imaginary part of the index of refraction was non-negligible, while the restrahlen bands showed continuous decrease in spectral contrast and some change in the shape of the bands with decreasing particle size, though the principal features diagnostic of composition were relatively unaffected. The transparency features showed several important changes with decreasing particle size: the spectral contrast increased then decreased, the position of the maximum reflectance of the transparency features shifted systematically to shorter wavelengths, and the symmetry of the features changed. Mie theory predicts that the extinction and scattering efficiencies should decline rapidly when particle size and wavelength are approximately equal. Using these relationships, a critical diameter where this change is predicted to occur was calculated as a function of wavelength and shown to be effective for explaining qualitatively the observed changes. Each of the mineral particle size series were then modeled quantitatively using Mie calculations to determine single-scattering albedo and a Hapke model to calculate reflectance. The models include the complex indices of refraction for olivine and quartz and the exact particle size

distributions. The olivine particle size series was well modeled by these calculations, and correctly reproduced the systematic changes in the volume scattering region, the Christiansen feature, restrahlen bands, and transparency features. The quartz particle size series were less well modeled, with the greatest discrepancies in the restrahlen bands and the overall spectral contrast. © 1997 Academic Press

## INTRODUCTION

One of the significant challenges to the use of reflectance and emission spectroscopy for the quantitative analysis of soil composition is separating the effects of particle size from composition. Studies using relative differences in spectral properties are often limited in the preciseness of statements regarding the degree of compositional differentiation between units because of uncertainties in particle size. Similarly, analytical approaches must contend with trade-offs between absorption and scattering properties and often rely on assumptions about particle size and particle size distributions. Weathering processes on most planetary bodies result in particulate surfaces typically dominated volumetrically by large particles but numerically by small particles. These fine particles dominate the spectral properties of natural particulate surfaces through the large increase in the relative geometric cross section of small vs large particles and the resulting increases in surface relative to volume scattering (Aronson and Emslie 1973, Salisbury and Wald 1992, Gaffey *et al.* 1993). Although many investigators have documented the effects of particle size on spectra (e.g., Lyon 1965, Hunt and Vincent 1968, Pieters 1983, Crown and Pieters 1987, Salisbury *et al.* 1992), these studies have focused on relative large particle sizes (e.g.,  $>50 \mu\text{m}$ ) or have examined only the bulk effects of particles  $<25 \mu\text{m}$  in size. There have been few systematic studies of the effects of very fine particles on reflectance spectra of typical geologic materials over the extended wavelength range from 0.3 to 25.0  $\mu\text{m}$ .

Moersch and Christensen (1995) present the most recent analysis of the effects of particle size on emissivity spectra in a study of quartz at wavelengths between 7 and 25  $\mu\text{m}$ . They used particle sizes ranging from as large as 277  $\mu\text{m}$  to the smallest size of  $\approx 15 \mu\text{m}$  and evaluated the effectiveness of a variety of analytical approaches to model the systematic changes observed in the emission spectra. They conclude that Mie theory is necessary to accommodate the smallest particle sizes, though none of the modeling approaches examined were entirely successful in duplicating all the systematics observed as a function of particle size. In addition, this study stopped short of working with particle sizes that are likely to dominate in many natural planetary surfaces, namely the particles  $< 25 \mu\text{m}$  in size. For example, the particle size range for dust and drift material on Mars is estimated to be  $\approx 0.1$  to 10  $\mu\text{m}$  (e.g., Christensen and Moore 1992), while the  $< 25 \mu\text{m}$  size fraction for typical lunar soils comprise roughly 10–20 weight percent of the total mass (Carrier *et al.* 1991). The optical dominance of this fine fraction was elegantly demonstrated in a study by Pieters *et al.* (1993) which showed that the reflectance spectra of mature lunar soils were largely controlled by the optical properties of the  $< 25 \mu\text{m}$  size fraction.

The results reported in this paper build upon the excellent studies of the effects of particle size on reflectance spectra summarized and extended by Moersch and Christensen (1995). We focus on particle size separates in 5- $\mu\text{m}$  increments between 0 and 25  $\mu\text{m}$  of two minerals, olivine and quartz, and use reflectance spectra over the wavelength range 0.3 to 25  $\mu\text{m}$ . This wavelength range is relevant to many current and planned planetary missions (e.g., the Thermal Emission Spectrometer (TES) on the Mars Global Surveyor (MGS), and the OMEGA visible to near-infrared imaging spectrometer on the Mars-96 mission). In addition, this combination of particle size and wavelength range allows the examination of transitions in scattering and absorption behavior as particle size varies from larger than, equal to, and less than the wavelength of the observations and with changes in the optical constants. The two mineral types were selected to compare the systematics in equivalent wavelength regions for materials of differing optical properties, and because reasonably accurate optical constants were available that could be used to evaluate scattering and absorption models.

### SAMPLE PREPARATION

The samples utilized in this investigation are a forsteritic olivine (Fo 94, determined by electron microprobe) from Jackson County, NC, and a single quartz crystal from Brazil. Preparation and separation of very fine particles is a difficult task. Contamination from the grinding medium is common, especially when using metallic parts, and making clean narrow separations of very fine particles is particu-

larly challenging. The bulk olivine sample was disaggregated using a mortar and pestle, and contaminants (minor pyroxene, serpentine, and Fe-oxides) were removed by hand through visual inspection using an optical microscope. Many of the olivine grains possessed a thin rind of serpentine which was removed through a repeated process of light grinding and sieving until all particles  $> 100 \mu\text{m}$  were visually clean. Subsequent examination of the particulate sample using a petrographic microscope showed that the samples contained little to no serpentine. Spectroscopic measurements, however, revealed a minor component of serpentine persisted. Nevertheless, this contaminate does not play a significant role in the analysis presented.

The clean olivine was then ground into a very fine powder using a mortar and pestle. The resulting powder was dry sieved through a 25- $\mu\text{m}$  sieve. The sample remaining in the sieve was placed into a small beaker and suspended in ethanol, and poured through the 25- $\mu\text{m}$  sieve into a catch basin. Sample that still remained in the sieve was rinsed with ethanol over the catch basin to remove any clinging fines. The material in both the sieve and the catch basin were allowed to dry, covered to prevent contamination by dust. The material left in the sieve was returned to the mortar for further grinding, and the material in the catch basin was added to the previously collected material collected. This process was repeated until 18 grams of clean olivine with particle size  $< 25 \mu\text{m}$  was acquired.

The 18 grams of sample was professionally sieved by the Gilson Company into five particle size separates at 5- $\mu\text{m}$  intervals (20–25, 15–20, 10–15, 5–10, and 0–5  $\mu\text{m}$ ). The size distributions of particles within each separate were determined using an Elzone 280 PC Particle Size Analyzer. This instrument determines the volume of particles in a sample and is calibrated prior to each use against spheres of known size (10 and 20  $\mu\text{m}$ ). The basic principal is that when the particles pass through the orifice, which has a specific size, they disturb an electric field across the orifice that is proportional to the volume of the spheres. For these measurements we used a 60- $\mu\text{m}$  orifice for the 0–5-, 5–10-, and 10–15- $\mu\text{m}$  separates of olivine and a 120- $\mu\text{m}$  orifice for the rest of the separates. The minimum size for which reliable measurements could be made was 1.6  $\mu\text{m}$  with the 60- $\mu\text{m}$  orifice and 4.9  $\mu\text{m}$  for the 120- $\mu\text{m}$  orifice.

The particle size distributions for the olivine separates are shown in Fig. 1 and summarized in Table I. The distribution of particles in each separate is approximately Gaussian, with distributions largely confined within the bounds of the individual sieve size. For the finest separate, the minimum size resolution of 1.6  $\mu\text{m}$  prevents the measurement of the smallest particles in this separate. However, it is evident that the peak of the particle size distribution was measured, as the volume percent rises from 1.6 to 3.0  $\mu\text{m}$ . This demonstrates that the sieving process pro-

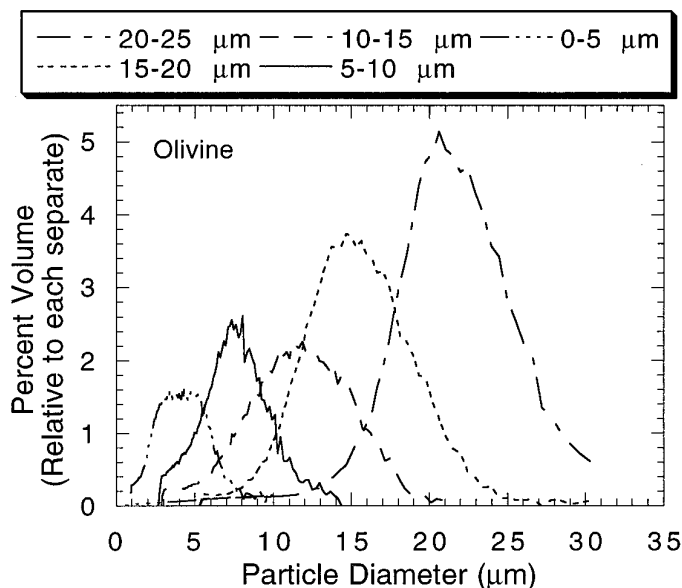


FIG. 1. Particle size distribution of olivine size separates, measured by an Elzone 280 PC particle size analyzer. The vertical axis shows frequency in normalized volume percent.

duced separates with very narrow size distributions that are necessary for this investigation. In addition, SEM micrograph images of the separates (Fig. 2) show that they are generally free of clinging fines, and therefore, the spectra of the samples are not expected to be significantly affected by particles with sizes outside the bounds of a given separate.

The quartz sample was prepared using the same methods as the olivine, beginning with a single, homogeneous crystal from Brazil. Utilizing the wet and dry sieving methods, seven different size separates were obtained ranging from 250–500  $\mu\text{m}$  to less than 25  $\mu\text{m}$ . The <25- $\mu\text{m}$  quartz powder was dry sieved using a Vibratory 3 inch Sieve Shaker and Muckbee Mears Micro Mesh Electroformed Sieves into five size separates from 25 to 0  $\mu\text{m}$  (<5  $\mu\text{m}$ , 5–10  $\mu\text{m}$ , 10–15  $\mu\text{m}$ , 15–20  $\mu\text{m}$ , and 20–25  $\mu\text{m}$ ).

The distribution of particles within the four of the five size separates were analyzed using an Elzone 280 PC Parti-

TABLE I

Sample separate	Volumetric mean particle size	Numeric mean particle size
00–05 $\mu\text{m}$	$4.58 \pm 2.78 \mu\text{m}$	$2.91 \pm 0.97 \mu\text{m}$
05–10 $\mu\text{m}$	$7.14 \pm 2.56 \mu\text{m}$	$4.79 \pm 1.85 \mu\text{m}$
10–15 $\mu\text{m}$	$10.62 \pm 3.59 \mu\text{m}$	$5.90 \pm 3.10 \mu\text{m}$
15–20 $\mu\text{m}$	$17.29 \pm 10.96 \mu\text{m}$	$11.50 \pm 3.99 \mu\text{m}$
20–25 $\mu\text{m}$	$29.46 \pm 15.91 \mu\text{m}$	$14.55 \pm 8.07 \mu\text{m}$

Note. Average particle sizes for the olivine size separates as measured using an Elzone 280 PC particle size analyzer.

cle Size Analyzer. Our attempts to measure the particle size distribution for the 0–5- $\mu\text{m}$  separate for quartz was unsuccessful due to excessive instrument noise. The results of this analysis are shown in Fig. 3, and are summarized in Table II. The size distribution of particles in the separates is largely Gaussian, though the distributions show a greater spread compared to the sieve separates obtained with the olivine (Fig. 3, Table II).

## MEASUREMENTS

Reflectance spectra of each size separate for the minerals olivine (Fig. 4) and quartz (Fig. 5) were measured with the NASA Reflectance Laboratory Facility at Brown University. This facility consists of two instruments, a bidirectional reflectance spectrometer, which was used in this investigation to cover the wavelength range 0.3 to 2.6  $\mu\text{m}$  (RELAB), and a Nicolet 740 FTIR Spectrometer for the wavelength range 0.9 to 25.0  $\mu\text{m}$ . The data from RELAB have excellent precision and accuracy and were therefore taken to be absolute reflectance. To facilitate examination across the entire wavelength range, the reflectance data obtained by the Nicolet spectrometer were scaled and merged with the RELAB data at 1.755  $\mu\text{m}$ . Because the reflectance attachment in the Nicolet (made by SpectraTech) has an on-axis biconical geometry, these measurements may be subject to highly localized non-lambertian effects which can cause differences in curve shape relative to measurements of diffuse reflectance, particularly in the region of the restrahlen bands (Salisbury *et al.* 1992).

These effects may be minimized through the use of sample collars to block strong, forward scattering first surface reflections, or through the use of careful and consistent sample preparations. For these measurements, we developed a consistent method of preparation to minimize the appearance of spurious features. The fine powders were poured into the sample dishes and gently tapped to induce settling. Once the sample dish was filled completely, the excess powder was removed by placing a straight edge along the top-left edge of the dish, angled slightly outward. This edge was then drawn across the dish, keeping the angle of the blade constant, which removed the excess powder. It was found that using the same procedure with the blade vertical, or angled in over the sample dish caused the surface of the sample to become packed. This results in an enhancement of the restrahlen bands and the appearance of spurious features, similar to those demonstrated with packed powders (Salisbury *et al.* 1992).

The objectives of this investigation are to make measurements and observations that allow insight into scattering and absorption by fine particles, which will ultimately have application in the analysis of data to be obtained of planetary surfaces by instruments such as the Thermal Emission Spectrometer (TES) on the Mars Global Surveyor space-

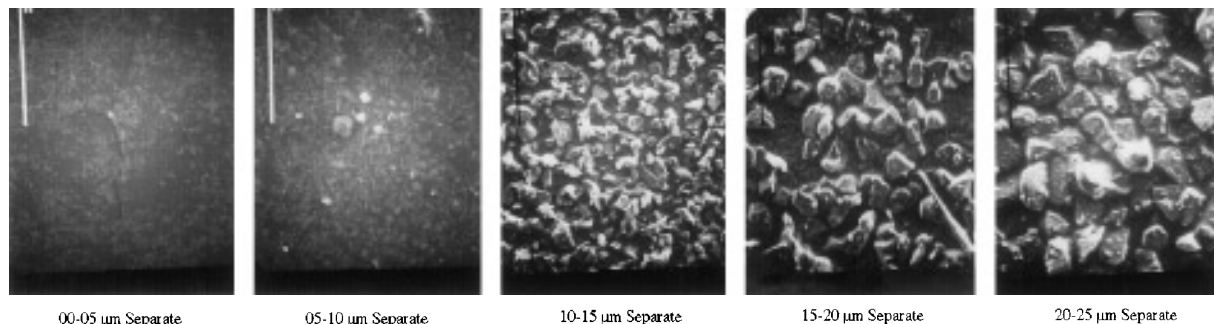


FIG. 2. Scanning electron micrograph images of olivine size separates. The scale bar in the upper left corner is 100  $\mu\text{m}$  in all five images.

craft (Christensen *et al.* 1992). Reflectance and emissivity are related by Kirchoff's law ( $R = 1 - \epsilon$ ), and thus the measurements presented here should be comparable to those obtained remotely. However, Salisbury *et al.* (1992) have stated that this relationship is only strictly true for emissivity and reflectance data integrated over all viewing geometries such as directional-hemispherical reflectance.

To assure that the data obtained with RELAB are directly relevant to emissivity spectra, the olivine samples were also measured using the directional-hemispherical Nicolet FTIR (DHR) spectrometer at Johns Hopkins University (Salisbury *et al.* 1992) and the Mattson Cygnus 100 FTIR emission spectrometer at Arizona State University (Christensen and Harrison 1993). The DHR spectrometer utilizes a liquid nitrogen cooled, mercury-cadmium-telluride (MCT) detector with a spectral resolution of

4  $\text{cm}^{-1}$ . The DHR configuration utilizes a 12.7-cm diameter sphere, internally coated with a diffusely reflecting gold surface, with a 2.5-cm diameter port  $10^\circ$  from the vertical to allow the source beam to enter and fall on a 2.5-cm sample/reference port at the base of the integrating sphere. The detector port is located at a  $90^\circ$  angle to the principal plane in the side of the sphere, and the MCT detector is baffled to eliminate direct viewing of either the sample or the specular "hot spot" on the sphere wall (Salisbury *et al.* 1992, Salisbury 1993). The emission spectra were measured with an uncooled Mattson Cygnus 100 FTIR spectrometer utilizing a KBr beamsplitter and a DTGS detector, with a spectral resolution of 4  $\text{cm}^{-1}$ . The spectrometer utilizes the heated sample, purged with  $\text{N}_2$  external to the spectrometer, as a source and an external mirror to direct the emitted energy into the spectrometer.

The spectra for all three systems over the wavelength range 6–26  $\mu\text{m}$  for the olivine separates are shown in Fig. 6.

## OBSERVATIONS

### Background

The principal focus of this work is to contrast absorption and scattering for fine particles in regions exhibiting volume scattering to the same processes in regions dominated

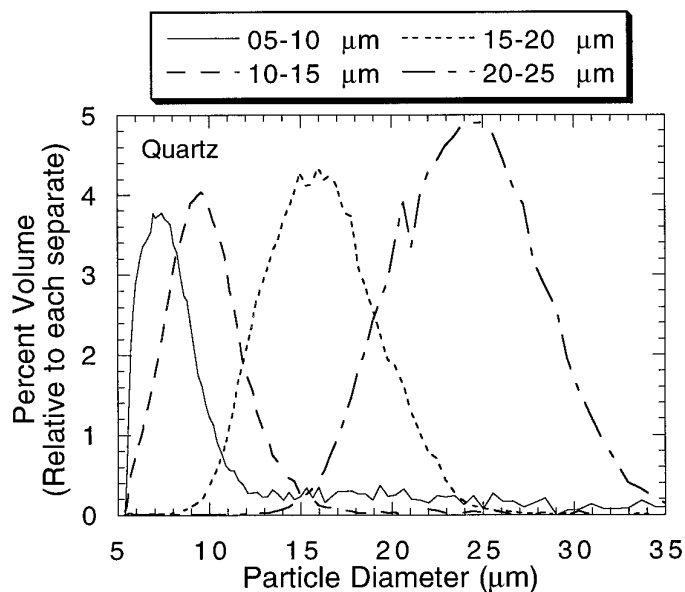


FIG. 3. Particle size distribution of four of the six less than 25- $\mu\text{m}$  quartz size separates, measured by an Elzone 280 PC particle size analyzer. The vertical axis shows frequency in normalized volume percent.

TABLE II

Sample separate	Volumetric mean particle size	Numeric mean particle size
00–05 $\mu\text{m}$	<sup>a</sup>	<sup>a</sup>
05–10 $\mu\text{m}$	$8.80 \pm 1.59 \mu\text{m}$	$7.10 \pm 1.53 \mu\text{m}$
10–15 $\mu\text{m}$	$9.53 \pm 2.44 \mu\text{m}$	$8.26 \pm 1.77 \mu\text{m}$
15–20 $\mu\text{m}$	$15.64 \pm 3.05 \mu\text{m}$	$13.79 \pm 3.02 \mu\text{m}$
20–25 $\mu\text{m}$	$23.78 \pm 4.57 \mu\text{m}$	$20.72 \pm 5.32 \mu\text{m}$

Note. Average particle sizes for the quartz size separates as measured using an Elzone 280 PC particle size analyzer.

<sup>a</sup> No distribution measured for this separate.

by restrahlen bands. Because the wavelength range investigated (0.3 to 25  $\mu\text{m}$ ) is comparable to the particle size at some wavelength in all the sample size separates, it is also possible to examine the effects on scattering and absorption as processes transition from the geometric optics regime ( $d \gg \lambda$ ) to the regimes where diffraction become important ( $d \approx \lambda$  and  $d < \lambda$ ). The spectral features in these data exhibit a number of different changes as a function of particles size. As has been noted by previous investigators, many of these changes can be qualitatively explained as due to the relative importance of surface reflection vs volume transmission, and ultimately are related to the complex index of refraction, defined by the optical constants  $n$  and  $k$  (e.g., Vincent and Hunt 1968, Hunt and Vincent 1968, Conel 1969, Salisbury and Wald 1992, Moersch and Christensen 1995). The optical constants for the two materials used in this study are shown in Fig. 7. The values for olivine are for a forsteritic olivine and are derived from Hiroi and Pieters (1994) for the wavelength region 0.3 to 2.6  $\mu\text{m}$  and Mukai and Koike (1990) for the wavelength region 7.0 to 25  $\mu\text{m}$ . For quartz,  $n$  and  $k$  are derived from the widely used dispersion parameters of Spitzer and Kleinman (1961) over the wavelength range 5 to 25  $\mu\text{m}$ . We adopt the convention of combining the ordinary and extraordinary rays for quartz in a 1/3–2/3 weighted average (e.g., Hapke 1981, Moersch and Christensen 1995) to approximate the relative contribution of each type of ray in a randomly oriented particulate surface.

Volume scattering refers to the optical processes that occur when  $k$  is small ( $\ll 1.0$ ) and  $n$  is greater than 1. Reflectance and absorption as a function of particle size generally follow a well recognized and studied trend. When particle sizes are large ( $\approx 250 \mu\text{m}$ ), reflectance is relatively low and absorptions are moderate. As particle size decreases, reflectance increases as the number of first-surface reflections and the amount of multiple scattering increases. When  $k$  is non-zero and varies as a function of wavelength, the absorption strength (defined as  $1 - R_b/R_c$ , where  $R_b$  is the reflectance at the band minimum and  $R_c$  is the continuum reflectance) initially increases with decreasing particle size to a point where the mean optical path length and the absorption path length ( $\approx \lambda/(4\pi k)$ ) are comparable (Hapke 1993). Further decreases in particle size result in a weakening of the absorptions. This behavior is well illustrated by the olivine crystal field absorptions between 0.6 and 1.5  $\mu\text{m}$  (Fig. 4) and the overtones and combination overtones of internal and lattice mode vibrations of both quartz and olivine between approximately 4 and 8  $\mu\text{m}$ . This has also been called class 3 (Moersch and Christensen 1995) or Type III (Vincent and Hunt 1968) behavior.

The restrahlen bands occur when  $k$  is large ( $>0.1$ ) such that very little energy passes through grain boundaries, and thus the scattering and absorption properties are controlled by first surface reflectance and multiple scattering.

This results in a maximum in reflectance and a minimum in emissivity. At large particle sizes, there is little multiple scattering and reflectance is a maximum. As particle size decreases such that the size is less than the wavelength, the particle as a whole interacts with a wavelength of light. In this regime, the decrease in scattering efficiency is proportional to  $1/(\lambda^4)$ , while the decrease in absorption efficiency is proportional to  $1/\lambda$  (Hapke 1993). Thus reflectance typically decreases and emissivity increases. This can be readily observed in the spectra of olivine near 10, 16, 18, and 24  $\mu\text{m}$ , and in quartz near 9, 13, and 20  $\mu\text{m}$ . In addition, the shape and strength of these features can be modified by small amounts of fine particles, present as clinging fines, which act to increase the amount of fine-particle volume scattering (Salisbury and Wald 1992). This has been termed class 1 (Moersch and Christensen 1995) or Type I (Vincent and Hunt 1968) behavior.

The principal Christiansen feature for quartz occurs near 7.5  $\mu\text{m}$  while for olivine it occurs near 9.0  $\mu\text{m}$ . The traditional definition of the Christiansen feature (e.g., Salisbury 1993) refers to the spectral feature that occurs when  $n = 1$  and  $k$  is small. Because  $n$  is equal to the refractive index of the medium (air), there is no reflection at grain boundaries and the radiation passes freely through the material without scattering and little absorption. This results in a minimum in reflectance and a maximum in emissivity. Recently, however, Hapke (1996) has proposed an alternative definition. He distinguishes between the Christiansen wavelength (where  $n = 1.0$ ) and the emissivity maximum, typically referred to as the Christiansen feature. The emissivity maximum is displaced to longer wavelengths from the Christiansen wavelength. It is located at the wavelength where particle scattering undergoes a transition from volume-scattering to surface-scattering, and is thus more a function of increasing  $k$  than the fact that  $n = 1$ .

Transitions between these different behaviors as a function of wavelength and the optical properties of the materials produce striking contrast reversals, best illustrated in the spectra of quartz (Fig. 5). Between 5 and 8  $\mu\text{m}$  the spectra exhibit classic class 3 behavior, with increases in reflectance as particle size decreases. As the optical properties transition through the Christiansen feature near 8  $\mu\text{m}$  to class 1 behavior, the largest particle size is the brightest, and reflectance decreases with decreasing particle size. Several similar such transitions are observed in the data out to 25  $\mu\text{m}$ . However, the relative changes as a function of particle size differ markedly, and this is due to the fact that the behaviors, and nature of the transitions between behaviors is governed by the specific values of the optical constants  $n$  and  $k$  relative to the dominant particle size of the materials and the wavelength observed. The coupling between absorption, scattering, wavelength, and particle size results in a continuous sequence of transitions between these behaviors.

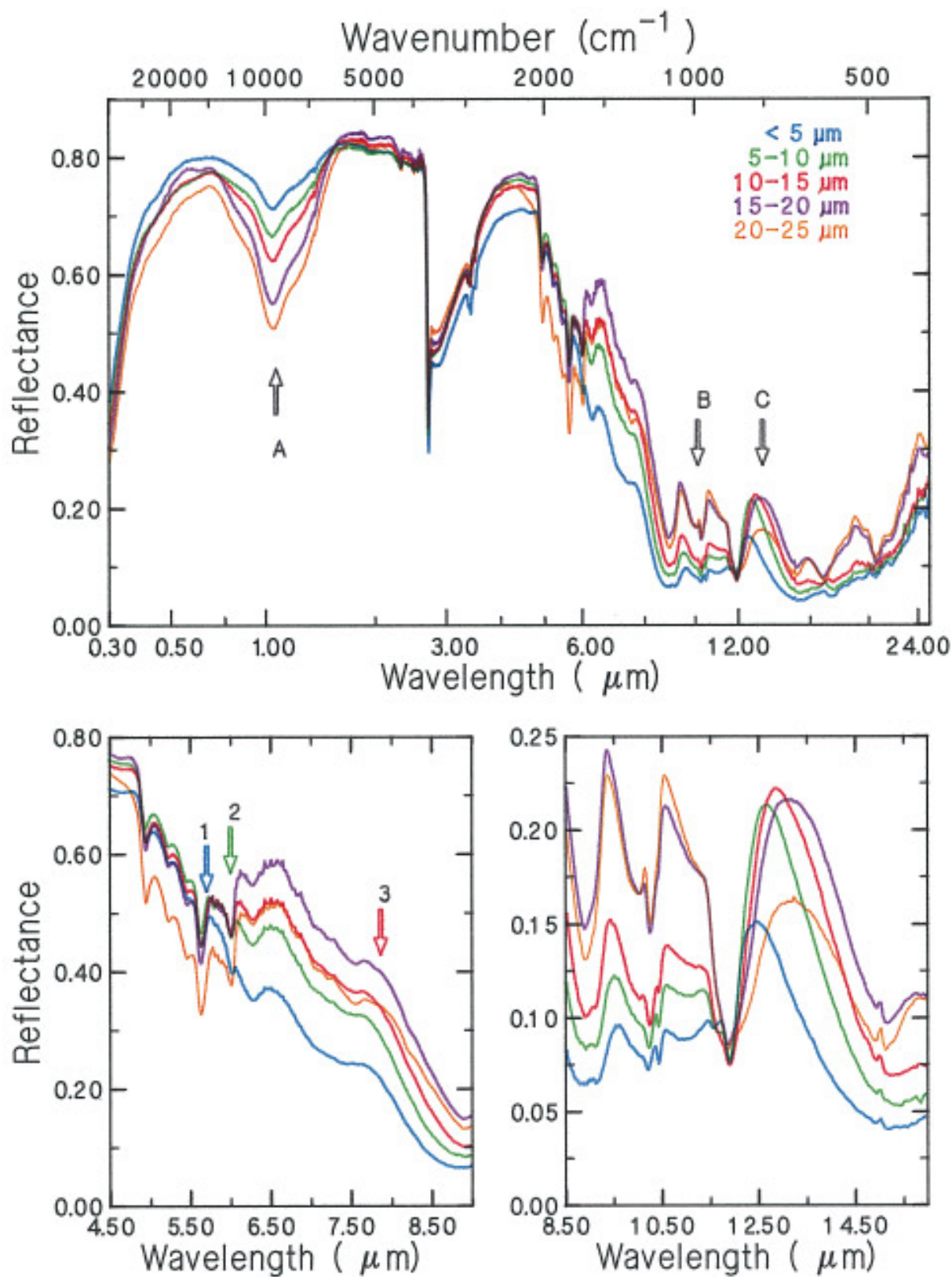


FIG. 4. Reflectance spectra over the extended wavelength range of 0.3 to 25.0  $\mu\text{m}$  of the olivine size separates. Note the changes, with particle size, in the crystal field absorptions (A), reststrahlen bands (B), and transparency feature (C).

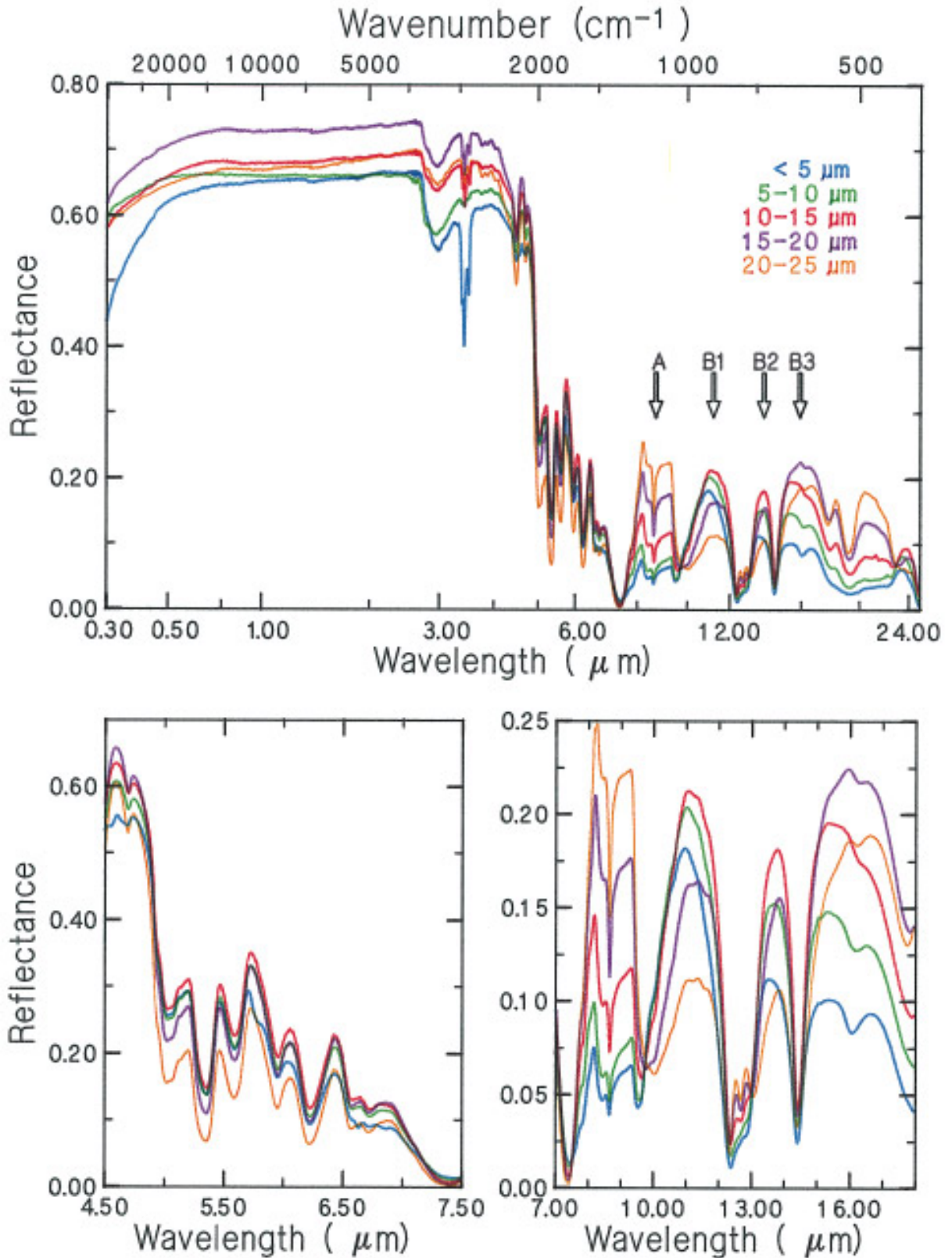


FIG. 5. Reflectance spectra over the extended wavelength range of 0.3 to 25.0  $\mu\text{m}$  of the quartz size separates (250–500  $\mu\text{m}$  to  $<25 \mu\text{m}$ ). Note the changes, with particle size, in the reststrahlen bands (A) and the transparency features (B1–B3).

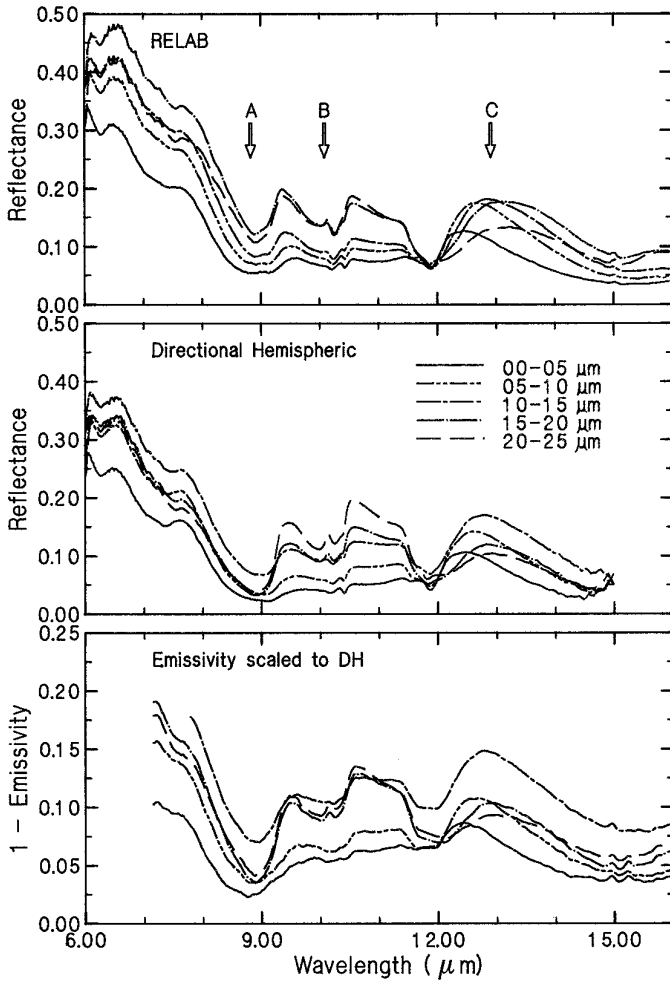


FIG. 6. Reflectance and emissivity spectra of the olivine separates over the wavelength region of 6 to 16  $\mu\text{m}$ . The top plot contains the RELAB spectra measured at Brown University, the middle contains Directional Hemispheric Reflectance (DHR) Spectra measured at Johns Hopkins University, and the bottom shows Emissivity Spectra (ES; converted to reflectance via Kirckoff's Law) measured at Arizona State University. Note the similar changes, with decreasing particle size, between the spectral sets in the Christiansen feature (A), restrahlen bands (B), and transparency feature (C).

#### Systematic Effects of Hyperfine Particles: RELAB Data

The systematics of reflectance as a function of particle size discussed above are generally relevant to particulate surfaces where the particles are large relative to the wavelength of light, or have particle size distributions that include both large and small particles. As noted above, these systematics have been confirmed by numerous investigations. What we have been able to do in this study is isolate narrow size separates for particles that are comparable to the wavelength of light in different wavelength regions from 0.3 to 25  $\mu\text{m}$ , depending on the separate. Through the use of two different materials, olivine and quartz, we

are also able to compare and contrast the effects of fine particles on materials of differing optical properties. The importance of these particle sizes is that for many planetary surfaces, some contribution from very fine particles is expected, ranging from complete dominance for dust deposits on Mars to a significant component of mature mare soils. In the following discussion, the principal effects of the hyperfine particles are described and summarized.

As particle size approaches the wavelength of light in the volume scattering regime (e.g., 0.3 to 8.0  $\mu\text{m}$  in quartz and olivine), the spectra exhibit a marked decline in reflectance and spectral contrast. This decline in reflectance is most readily observed in the spectra for olivine shown in Fig. 4. From 0.3  $\mu\text{m}$  to approximately 1.5  $\mu\text{m}$ , the 0–5  $\mu\text{m}$  separate is the brightest separate. Between 1.5  $\mu\text{m}$  and 5.5  $\mu\text{m}$ , the reflectance of this separate is slightly lower than or comparable to the reflectance of the other separates.

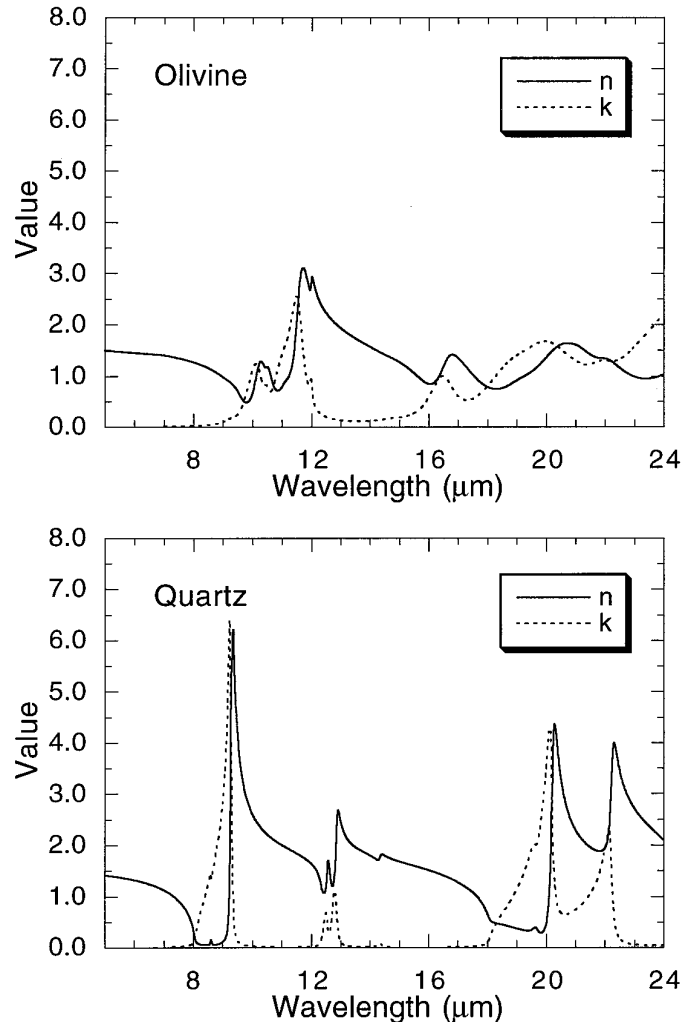


FIG. 7. The real ( $n$ , dash-dot line) and imaginary ( $k$ , solid line) parts of the complex index of refraction for olivine (top) and quartz (bottom).

However, beginning at  $5.5\ \mu\text{m}$ , the reflectance exhibits a sharp decline such that it is significantly lower than all the other separates. A distinct decline in intensity is also observed in the other separates and can be characterized by “cross-overs” between the spectra. This is defined as the wavelength where the spectrum of a given size separate decreases sharply to “cross” the reflectance spectrum of the next largest size separate. For example, as the wavelength of light increases relative to the average particle size of the  $0\text{--}5\text{-}\mu\text{m}$  separate ( $\langle D \rangle 2.915\ \mu\text{m}$ ) to the point where the wavelength is now greater than the average particle size, the reflectance decreases and crosses the spectrum of the  $5\text{--}10\text{-}\mu\text{m}$  separate at  $\approx 5.5\ \mu\text{m}$ . Such “cross-overs” have been observed for the  $0\text{--}5\text{-}$ ,  $5\text{--}10\text{-}$ ,  $10\text{--}15\text{-}$ , and  $15\text{--}20\text{-}\mu\text{m}$  separates near  $5.5$ ,  $6.00$ ,  $7.8$ , and  $8.50\ \mu\text{m}$ , respectively (Figs. 4 and 6). Although these effects are less evident in the spectra for quartz (Fig. 5), the reflectance of the finest separate ( $0\text{--}5\ \mu\text{m}$ ) does exhibit a cross-over near  $5.5\ \mu\text{m}$ .

In the spectra of olivine, the Christiansen feature (Figs. 4 and 6) near  $9.0\ \mu\text{m}$  appears to saturate, becoming deeper and broader toward both shorter and longer wavelengths, with decreasing particle size. The restrahlen bands between  $9\ \mu\text{m}$  and  $12\ \mu\text{m}$  exhibit both a reduction in spectra contrast (Lyon 1964, Vincent and Hunt 1968) and a change in shape (Salisbury and Wald 1992) as particle size decreases (Figs. 4 and 6). For the  $15\text{--}20\text{-}\mu\text{m}$  separate, the restrahlen peak at  $9.5\ \mu\text{m}$  is stronger than the peak at  $11.0\ \mu\text{m}$ . As particle size decreases, the peak at  $9.5\ \mu\text{m}$  exhibits a slightly larger decrease in contrast than the peak at  $11.0\ \mu\text{m}$ , so that in the  $0\text{--}5\text{-}\mu\text{m}$  separate the peak at  $11.0\ \mu\text{m}$  is stronger than the peak at  $9.5\ \mu\text{m}$ . In addition, the peak at  $11.0\ \mu\text{m}$  exhibits a change in shape such that the peak flattens out. It is important to note, however, that despite the changes in contrast and shape, the wavelength positions are apparently unaffected by changes in particle size.

The spectra for quartz show essentially identical behavior, except that the Christiansen feature does not saturate to the same degree as observed in olivine. The change in shape of the restrahlen peaks between  $7.5$  and  $9.5\ \mu\text{m}$  follows an evolutionary path where the second peak begins as a relatively symmetric, rounded feature in the larger particle sizes and becomes asymmetric in the smaller particle sizes, sloping upward toward longer wavelengths. This is contrasted with the first peak which begins asymmetric sloping upward in the larger particle sizes and ends sloping downward toward longer wavelengths in the smaller particle sizes.

A small number of features in these spectra (Figs. 4 and 5) vary in wavelength position as a function of particle size. The transparency features (Salisbury and Wald 1992, Salisbury and Walter 1989) near  $13\ \mu\text{m}$  in olivine (Fig. 6) and near  $11$ ,  $14$ , and  $16\ \mu\text{m}$  in quartz (Fig. 5) are the most notable. The transparency feature in olivine exhibits

a systematic shift in the position of peak reflectance to shorter wavelengths, a systematic increase then decrease in peak reflectance, and an increasingly asymmetric shape as particle size decreases. In the largest size separate ( $20\text{--}25\ \mu\text{m}$ ), the peak reflectance is located at  $13.22\ \mu\text{m}$ , and shifts to  $12.46\ \mu\text{m}$  in the smallest separate ( $0\text{--}5\ \mu\text{m}$ ). The peak reflectance of the transparency feature increases, as particle size decreases, from  $13.36\%$  reflectance in the  $20\text{--}25\text{-}\mu\text{m}$  separate to a maximum of  $18.13\%$  reflectance in the  $10\text{--}15\text{-}\mu\text{m}$  size range. As particle size continues to decrease, the peak reflectance of the feature begins to decrease to  $12.61\%$  reflectance (Fig. 6).

For the  $11\text{-}\mu\text{m}$  transparency feature in quartz, the reflectance increases from the  $20\text{--}25\text{-}$  to the  $15\text{--}20\text{-}\mu\text{m}$  separate, though the wavelength of the maximum reflectance is relatively constant near  $11.5\ \mu\text{m}$ . For the  $10\text{--}15\text{-}$  and  $5\text{--}10\text{-}\mu\text{m}$  separates, the reflectance continues to increase, but the wavelength of maximum reflectance is shifted to  $11.0\ \mu\text{m}$ . For the smallest separate ( $0\text{--}5\ \mu\text{m}$ ), the reflectance decreases, though the wavelength of maximum reflectance is still  $11.0\ \mu\text{m}$ . Simultaneously, the symmetry of the transparency feature changes systematically from large to small particle size separates as a greater increase in reflectance is exhibited in the  $9.5\text{--}11\text{-}\mu\text{m}$  wavelength region for each successively smaller separate. Essentially identical behavior is exhibited for the transparency feature near  $14\ \mu\text{m}$ . For the  $16\text{-}\mu\text{m}$  feature, the maximum reflectance is exhibited by the  $15\text{--}20\text{-}\mu\text{m}$  separate, with systematic decreases in reflectance and increases in asymmetry for the smaller separates.

#### *Comparison and Contrast of Measurement Sets (Olivine)*

As noted above, spectra were obtained for the suite of olivine separates using the RELAB spectrometers, the DHR facility at Johns Hopkins University, and emission spectra from the facility at Arizona State University (Fig. 6). This set of measurements allows us to compare observed features of, and changes in the spectra as particle size decreases. In general, the spectra from all three instruments exhibit the same fundamental features as a function of decreasing particle size: (1) sharp decrease in reflectance for the smallest separate in the  $5\text{--}8\text{-}\mu\text{m}$  wavelength region when the wavelength becomes comparable to average particle diameter; (2) saturation of the Christiansen feature in the finest separates; (3) decrease in strength and change in shape of the restrahlen band; and (4) changes in strength, shape, and position of the transparency feature. However, differences within the spectra obtained in the different systems have been noted. The differences in the spectral measurement sets occur in the Christiansen feature and the restrahlen band. For the DHR and emissivity spectra (Fig. 6), the  $10\text{--}15\text{-}\mu\text{m}$  separate is the brightest, the  $0\text{--}5\text{-}\mu\text{m}$  is the darkest, and the spectra of the  $5\text{--}10\text{-}$ ,  $15\text{--}20\text{-}$ ,

and 20–25- $\mu\text{m}$  separates are closely spaced within the Christiansen feature. In the RELAB spectra, the 0–5- $\mu\text{m}$  separate is the darkest, while the 15–20- $\mu\text{m}$  separate is the brightest, and there is a separation of a few percent (reflectance) between the spectra in the Christiansen feature. Within the restrahlen band, the restrahlen peak at 9.5  $\mu\text{m}$  has a lower reflectance than the peak at 11  $\mu\text{m}$  in the DHR and emission spectra (Fig. 6). The RELAB spectra of this same spectral region display differences in the relative strengths of the two peaks. As particle size decreases, the shape of the second peak of the restrahlen band changes. The side to shorter wavelengths decreases more than the side to longer wavelengths, resulting in the flattening of the peak into more of a plateau. This change is more dramatic in both the directional hemispheric reflectance spectra and thermal emission spectra where the overall slope of the peak reverses. The causes of these minor differences are not understood, but may be due to non-uniform scattering, differences in sample preparation, or measurement geometry. Nevertheless, all three suites of spectra exhibit the same important changes of intensity and contrast, and therefore the changes in spectral properties are due primarily to decreasing particle size and are not a result of sample preparation and/or instrumentation.

#### A THEORETICAL BASIS: MIE THEORY

The qualitative effects of the transition from large to fine particles on reflectance spectra described above are evident, repeatable between different types of measurements (e.g., reflectance and emissivity), and exhibit similar behavior in materials of different optical properties, though some of the details are different. The objective in this section is to develop an understanding of the causes of these systematics in the reflectance spectra. Most reflectance models for planetary surfaces are based on geometric optics, where the particle size is larger than the wavelength of light, and are thus not directly applicable to these measurements. The most well-studied and developed theoretical treatment of scattering by small particles is Mie theory. Mie theory is only strictly valid for smooth particles separated by at least three radii, and has been widely used in the study of planetary and stellar atmospheres. However, Conel (1969) developed a “dense atmosphere” model based on Mie theory that was applied to laboratory measurements of emissivity from particulate surfaces, which showed a reasonable first-order agreement between the model and measurements. More recently, Moersch and Christensen (1995) presented an evaluation of several models for emissivity and concluded that Mie calculations for single-scattering that are then used in a multiple-scattering emission model (Hapke, 1993) provides the best fit of model calculations to observed emissivity measurements of quartz. However, they note some important discrepan-

cies, particularly for the restrahlen bands, which they believe is in part due to errors in the published values for the optical constants of quartz. Wald and Salisbury (1995) have also questioned the validity of these optical constants and present evidence to indicate that there is some error in the values, and these discrepancies are likely to have the greatest impact on the modeling of fine particles.

In the following discussion, we first use Mie theory as a tool to qualitatively understand the systematic effects observed in the spectra of fine particle separates. We then follow with a hybrid Mie–Hapke scattering model, similar to that proposed by Moersch and Christensen (1995) for emissivity, but for reflectance in our case.

Two parameters control the results of calculations based on Mie theory: the ratio of the particle size to the wavelength, and the refractive index of the particle relative to the surrounding medium ( $m = n + ik$ ). The ratio of particle size, referred to as the *size parameter*, to wavelength is usually expressed as  $X = \pi D/\lambda$ , where  $D$  is the diameter of the particle and  $\lambda$  is the wavelength. The solutions of Mie theory have different properties depending on how the value of the size parameter compares to unity. Hapke (1993) defines three different scattering regimes based on this parameter: Raleigh, where  $X \ll 1$ ; Mie (or resonance), where  $X \sim 1$ ; and Geometric-optics, where  $X \gg 1$ . Our investigation focuses on the resonance regime.

Mie theory provides us with a tool for understanding the effects of decreasing particle size on reflectance spectra. When the parameter  $(n - 1)X$  (where  $n$  is the real part of the complex index of refraction and  $X$  is the relation between particle size ( $2\pi r$ ) and wavelength) is approximately 2, the extinction efficiency reaches a maximum. The fact that the maximum value of  $Q_e$  exceeds unity simply means that the region of the wave front affected by the particle is larger than the physical size of the particle, largely due to diffraction. If  $(n - 1)X$  is less than approximately 2, then the extinction efficiency ( $Q_e$ , equal to the sum of the efficiency of scattering and absorption) experiences a rapid decline (c.f. Hapke 1993). This occurs when the particle size is less than the wavelength, and the interaction between any given particle and the advancing wave front decreases rapidly with size. It follows that because  $Q_e$  declines rapidly with decreasing particle size, so must the scattering and absorption efficiencies. However, scattering efficiency declines more rapidly than absorption efficiency, resulting in a net decrease in the single scattering albedo, independent of the optical properties for  $k < 0.1$ .

It is worthwhile to consider why scattering efficiency declines more rapidly than absorption efficiency. Essentially, as the particles become smaller than the wavelength, and  $Q_e$  declines, the scattering efficiency will become less because the effective cross section of the grains is reduced and the particle interacts with an entire wavelength of light. As mentioned earlier, scattering efficiency decreases as

$1/(\lambda^4)$ , but absorption efficiency declines as only  $1/(\lambda)$ . Thus the light can penetrate further into the particulate medium, increasing the effective optical depth of the particulate surface. This will cause the bulk absorbing properties of the medium to increase in a relative sense. The net result is an overall lowering of the reflectance due primarily to non-selective absorption. This is best illustrated by the reflectance spectrum of the 0–5- $\mu\text{m}$  separate of olivine shown in Fig. 4. It is comparable in reflectance to the 5–10- and 10–15- $\mu\text{m}$  separates between 5 and 6  $\mu\text{m}$ . Then as the reflectances of the other separates increase to a reflectance peak near 6.2  $\mu\text{m}$ , the reflectance of the 0–5- $\mu\text{m}$  separate shows a sharp decline.

These same systematics do not hold when the imaginary index of refraction,  $k$ , is large. When  $k$  is large ( $>1$ ), there is no simple relationship between  $Q_c$  and the size parameter (Bohren and Huffman 1983).  $Q_c$  is largely dependent on  $k$  in these situations. The observed changes in the spectra of the fine particle size separates follow that expected for an increased importance of volume scattering as particle size decreases (Salisbury and Wald 1992).

We can therefore use the relationship that the extinction efficiency rapidly decreases as the parameter  $(n - 1)X$  becomes increasingly smaller than approximately 2 to define a critical particle diameter ( $D_c$ ) as a function of wavelength where a sharp decline in reflectance should occur.  $D_c$  is defined by

$$D_c = \frac{2\lambda}{\pi(n - 1)}. \quad (1)$$

This is calculated for olivine using the optical constants for olivine (Fig. 7) and the result is presented in Fig. 8. When a majority of particles in a separate are less than the critical diameter (e.g., below the solid line in Fig. 8), the extinction efficiency ( $Q_c$ ) should be reduced by a factor of 2 or more. It is important to note here that this value of  $D_c$  is only valid when  $k$  is small. For that reason we have not plotted the values of  $D_c$  in the restrahlen bands. Utilizing the calculation of  $D_c$  for olivine and the average particle size of the separates it is possible to understand the changes in the features within the spectra, over the wavelength range of 6 to 15  $\mu\text{m}$ , as a function of decreasing particle size. The principal consequences of this relationship for several specific wavelength regions are discussed below.

### Olivine

**6–9  $\mu\text{m}$  region: Volume scattering.** According to conventional geometric-optics ( $X \gg 1$ ; Hapke 1993), the 0–5- $\mu\text{m}$  separate should have the highest reflectance in this wavelength range. However, the opposite is observed. This is supported by the Mie calculations for the critical diam-

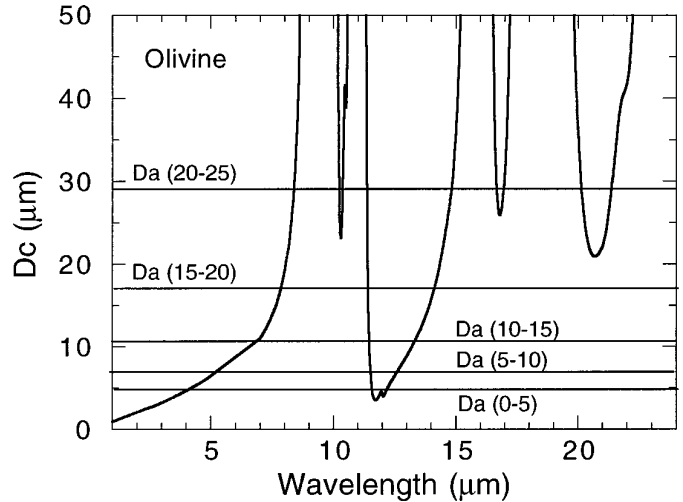


FIG. 8. Plot of the critical diameter ( $D_c$ ) of olivine over the wavelength range of 6 to 25  $\mu\text{m}$ . The region below this curve is where the extinction efficiency experiences a rapid decline, and hence reflectance is dramatically decreased. Horizontal lines represent the average particle size ( $D_a$ ) of the less than 25- $\mu\text{m}$  size separates.

ter ( $D_c$ ) of olivine and the volumetric mean (or average) particle size ( $D_a$ ) of the separate (Fig. 8), with the former being larger than the latter over the entire wavelength range of 6 to 9  $\mu\text{m}$ . The  $D_a$  of the 0–5  $\mu\text{m}$ -separate becomes smaller than  $D_c$  near 4  $\mu\text{m}$  (Fig. 8). By 6  $\mu\text{m}$ , the majority of the particles in the separate are less than  $D_c$  and the extinction efficiency of the spectra experiences a rapid decline which correlates to a decline in reflectance.

The RELAB spectrum of the 10–15  $\mu\text{m}$  (Fig. 6) shows a rapid decline in reflectance, such that it becomes darker than the 20–25- $\mu\text{m}$  separate near 8  $\mu\text{m}$ . This is consistent with  $D_c$  and  $D_a$ , in that  $D_a$  becomes smaller than  $D_c$  (Fig. 8) near 7  $\mu\text{m}$ . This results in the rapid decline in extinction efficiency, after approximately 7  $\mu\text{m}$  in wavelength, which leads to a progressive decline in reflectance as wavelength increases.

**Christiansen feature.** The average particle size of all of the separates is smaller than the critical diameter for olivine at the wavelength of the Christiansen feature ( $\sim 9.0$   $\mu\text{m}$ ; Figs. 6 and 8). The  $D_a$  of the 0–5- $\mu\text{m}$  separate is less than the  $D_c$  at a wavelength that is well before the Christiansen feature. The separate should exhibit the largest decrease in extinction efficiency ( $Q_c$ ), and in the Christiansen feature this would be expressed as both a decrease in reflectance within the feature and a widening of the feature. The  $D_a$  of the 20–25- $\mu\text{m}$  separate becomes smaller than the  $D_c$  of olivine near a wavelength of approximately 8.5  $\mu\text{m}$ . Because of this, the extinction efficiency of the separate decreases, but not to nearly the same degree as the  $Q_c$  of the 0–5- $\mu\text{m}$  separate. Since  $k$  is not negligible at the Christiansen Feature ( $\approx 0.1$ ), the reflectances exhibit

a combination of both volume scattering and Restrahlen behavior. This explains both the broadening of the feature, and the increase in reflectance for the larger particle size separates (e.g., Hapke 1996).

*9–12- $\mu\text{m}$  region: Restrahlen bands.* The changes that are observed in these bands are not simply understood from the perspective of  $D_c$  and  $D_a$ . This is because of the large value of  $k$  (Fig. 7) in this wavelength region. Salisbury and Wald (1992) demonstrated that the reduction in contrast and change in band shape in the restrahlen bands as a function of decreasing particle size are due primarily to the increasing importance of volume scattering. When the particles are large, first surface reflections due to large values of  $k$  dominate the observed reflectance measurements and the reflectances are high. As the particle size decreases, the increase in volume scattering allows a greater proportion of light to be transmitted across the grain boundaries where it is absorbed, thereby decreasing the measured reflectance. The change in shape of the features occurs as a result of the relative contributions to the reflectance from  $n$  and  $k$ . The peaks in the plot of  $k$  vs  $\lambda$  (Fig. 7) are shifted approximately  $0.25 \mu\text{m}$  to shorter wavelengths from the peaks in the  $n$  spectrum. Thus the wavelength regions where  $k$  is larger than  $n$  exhibit a larger decrease in reflectance as a function of decreasing particle size than vice versa which results in a change in shape, as well as spectral contrast, as a function of particle size.

*12–15- $\mu\text{m}$  region: Transparency feature.* The systematics in this region are analogous to those described for the volume scattering regime, except that the reflectance spectra are undergoing a transition from restrahlen to volume scattering on the short wavelength side of the feature. As in the 6–9- $\mu\text{m}$  region, the 0–5- $\mu\text{m}$  separate should be the brightest and the 20–25- $\mu\text{m}$  separate should be the darkest. In addition, Salisbury and Walter (1989) proposed that the wavelength of the reflectance peak of the transparency feature is diagnostic of composition and thus should remain constant. As demonstrated quite clearly in Fig. 6, the wavelength position of this feature is not constant. The reason for this is easily understood in the context of  $D_c$  and  $D_a$  shown in Fig. 8.

The average particle size of the 20–25- $\mu\text{m}$  separate becomes smaller than the critical diameter of olivine at a wavelength of approximately  $15.5 \mu\text{m}$  (Fig. 8). This is past the wavelength region of the transparency feature (Fig. 6), and hence the peak of the transparency feature (which, for the purpose of the rest of this discussion, will be the peak reflectance of the 20–25- $\mu\text{m}$  separate at  $13.22 \mu\text{m}$ ; Fig. 6). This means that the spectrum of the separate in this wavelength region does not experience a decline in extinction efficiency, resulting in a fully formed, fairly symmetric transparency feature consistent with previous measurements of olivine (Salisbury *et al.* 1992).

The average particle size of the 0–5- $\mu\text{m}$  separate becomes smaller than the critical diameter at a wavelength of approximately  $12.33 \mu\text{m}$  (Fig. 8), well before the peak reflectance of the transparency feature. This results in a strong decline in extinction efficiency over most of the wavelength region, from  $12.6$  to  $15.0 \mu\text{m}$ . This decline in extinction efficiency becomes greater as the wavelength increases, causing a progressively stronger decrease in reflectance across this wavelength region. This results in an asymmetric decrease in reflectance across the transparency feature, causing the peak of reflectance to shift to  $12.46 \mu\text{m}$ , and the overall shape of the transparency feature to become very asymmetric (Fig. 6).

The average particle size of the intervening separates becomes smaller than the critical diameter at shorter wavelengths as particle size decreases (Fig. 8). This results in an increasingly larger fraction of the wavelength region of the transparency feature to be a region of rapidly declining extinction efficiency, causing the peak reflectance of the feature to shift toward shorter wavelengths (Fig. 6). In the 10–15- $\mu\text{m}$  separate, this region of declining extinction efficiency covers only the latter half of the wavelength region of the transparency feature. This allows the 10–15- $\mu\text{m}$  separate, and the larger separates to behave primarily as they would be expected to behave in the geometric-optics regime, namely smaller size separates are brighter and the feature grows symmetrically. However, the declining extinction efficiency in the long wavelength tail of the transparency features decreases the reflectance in that region of the feature, causing a shift in the peak reflectance of the transparency feature to shorter wavelengths (Fig. 6). For smaller size separates, the wavelength region of the transparency feature that is affected by declining extinction efficiency increases to the point where the peak of the transparency feature (as described above) is experiencing a rapid decline in extinction efficiency. This results in the peak reflectance of these separates to become increasingly darker as particle size decreases (Fig. 6).

### Quartz

A similar analysis of the effects of declining  $Q_c$  on the reflectance spectra of quartz is discussed below. The critical diameter for quartz is calculated from the optical constants shown in Fig. 7.  $D_c$  as a function of  $\lambda$  is presented in Fig. 9.

*5.5–7.5- $\mu\text{m}$  region: Volume scattering.* The 0–5- $\mu\text{m}$  separate exhibits a decline in reflectance in this wavelength region. This is supported by the  $D_c$  shown in Fig. 9 that indicates that the majority of particles in this separate should be less than the critical diameter. The lack of change in reflectance for the other separates, though predicted by the  $D_c$  calculations, may be due to discrepancies in the optical constants of quartz (Wald and Salisbury 1995, Moersch and Christensen 1995) or the fact that  $n$  is close

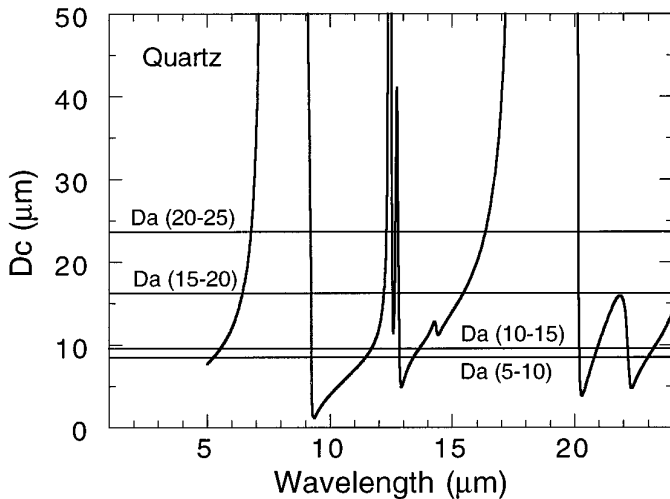


FIG. 9. Plot of the critical diameter ( $D_c$ ) of quartz over the wavelength range of 6 to 25  $\mu\text{m}$ . The region below this curve is where the extinction efficiency experiences a rapid decline, and hence reflectance is dramatically decreased. Horizontal lines represent the average particle size ( $D_a$ ) of the less than 25- $\mu\text{m}$  size separates.

to 1 in this wavelength region and our simple explanation may not apply in these situations.

**Christiansen feature.** The Christiansen feature in the quartz separates shows very little change with particle size. This is likely due to the fact that  $k$  is very small, and therefore we see none of the effects of the restrahlen-type behavior modulated by volume scattering observed in the spectra of the olivine separates. However, because  $n$  approaches, and becomes less than 1.0 near 12.25  $\mu\text{m}$ , a Christiansen feature is predicted at this wavelength. Indeed, the reflectances become very small at this point, but in this case the feature becomes broader to both short and long wavelengths, and the reflectance of the finest separate is the least, followed by the 5–10- and 0–10- $\mu\text{m}$  separates. This is directly comparable to the evolution of the Christiansen feature in olivine as a function of particle size. As seen in Fig. 7,  $k$  is rather large and increasing near 12.25, confirming the concept that volume scattering is contributing to the evolution of this feature.

**9–12- $\mu\text{m}$  region: Restrahlen bands.** The changes that are observed in these bands as a function of particle size are exactly analogous to those observed in the spectra of olivine. There is a complex interplay between  $n$ ,  $k$ , and the particle size, driven primarily by volume scattering. As volume scattering increases, larger decreases in reflectance due to  $k$  result. Since  $k$  is sloping upward from 8.0 to 9.25  $\mu\text{m}$ , this causes there to be an evolution in the shape of the restrahlen peaks to also have a sloping upward reflectance as particle size decreases. This is partially offset in the wavelength region between the Christiansen feature

( $\approx 7.5 \mu\text{m}$ ) and 8.25  $\mu\text{m}$  by the steadily decreasing value of  $n$ . As  $n$  decreases, the reflectance in the restrahlen bands increase, which offsets the increased absorption due to volume scattering. However, beyond 8.25  $\mu\text{m}$ ,  $n$  is small and relatively constant, and the spectral shape evolves primarily driven by the increasing value of  $k$  and the increase in volume scattering as particle size decreases.

**9.5–17.5- $\mu\text{m}$  region: Transparency features.** The three transparency features observed in the reflectance spectra of quartz in this wavelength region ( $\approx 11 \mu\text{m}$ ,  $\approx 13.5 \mu\text{m}$ , and  $\approx 16.5 \mu\text{m}$ ) provide an excellent test of this qualitative analysis of the relationship between  $D_c$  and  $D_a$  on the reflectance spectra. As shown in Fig. 9,  $D_c$  increases steadily from short to long wavelengths across each of the wavelength regions for these features. However, the intersection of  $D_a$  with  $D_c$  varies with each feature.  $D_c$  is less than  $D_a$  for most separates across most of the wavelength range of the 11- $\mu\text{m}$  feature,  $D_c$  is greater than  $D_a$  for the two smaller separates approximately half-way across the 13.5- $\mu\text{m}$  feature, and  $D_c$  is greater than  $D_a$  for the two smaller separates for most of the 16.5- $\mu\text{m}$  feature and for approximately half of the feature for the 15–20- $\mu\text{m}$  separate.

Examination of the spectra of the less than 25  $\mu\text{m}$  size separates (Fig. 5) shows that changes in the transparency features with decreasing particle size are consistent with the relationships between  $D_c$  and  $D_a$  described above. The transparency feature at 11  $\mu\text{m}$  exhibits only minor changes in symmetry and position of the peak reflectance. The maximum reflectance of the feature increases as a function of particle size, and only exhibits a decrease in reflectance, with a change in asymmetry on the long wavelength side of the feature, in the finest separate (Fig. 5). In contrast, the transparency feature at 14  $\mu\text{m}$  begins to exhibit a change in the symmetry of the transparency feature in the 5–10- $\mu\text{m}$  separate, and a sharp decrease in reflectance and increased asymmetry in the reflectance of the 0–5- $\mu\text{m}$  separate. The transparency feature at 16  $\mu\text{m}$  exhibits strong changes in symmetry, strength, and position of the peak reflectance. The peak reflectance of the feature reaches a maximum in the 15–20- $\mu\text{m}$  separate, and the wavelength position of the peak reflectance exhibits a strong shift from 16.62 to 15.36  $\mu\text{m}$  (Fig. 5). This is predicted from the plot of  $D_c$  and  $D_a$ , where  $D_a$  is smaller than  $D_c$  across the entire feature for the smallest separates, and about half the feature for the 15–20- $\mu\text{m}$  separate.

## REFLECTANCE MODELS

The qualitative analyses described above indicate that basic concepts of Mie theory for particle sizes that are comparable to the wavelength allow useful insight into the effects of fine particles on reflectance spectra. The recent work of Moersch and Christensen (1995) showed that Mie theory, when used in combination with a Hapke radiative

transfer model, provided the best approximation to their measured emissivity spectra. We use a similar approach here to assess the validity of this approximation for fine particle reflectance spectra.

Computer code presented by Bohren and Huffman (1983) was used to calculate scattering efficiency ( $Q_s$ ) and extinction efficiency ( $Q_e$ ) for homogeneous spheres. This code was modified to calculate  $Q_s$  and  $Q_e$  for  $n$  and  $k$  as a function of wavelength for any mineral, and to explicitly calculate these efficiencies for particle size distributions. The particle size distributions (Figs. 1 and 3) are normalized such that the sum of the frequencies equals one.  $Q_s$  and  $Q_e$  are calculated for each particle size interval, then multiplied by the normalized frequency, and summed over all particle size intervals. One of the properties of the Mie solution for  $Q_e$  as a function of the size parameter when the particles are similar in size to the wavelength and  $k$  is small ( $<0.1$ ) is a series of oscillations about a mean value of  $Q_e \approx 2.0$ . There is a long frequency component due to interference and a short-frequency ripple structure due to diffraction. Though these effects are pronounced for particles of a single size, they become averaged out in materials with particle size distributions (Bohren and Huffman 1983).

The Mie single-scattering albedo is then calculated from the ratio of  $Q_s$  to  $Q_e$ . To calculate reflectance, a simplified version of Hapke's (1981) equations for radiance coefficient is used. Radiance coefficient is the ratio of the radiance from the sample to the radiance of a 100% reflective lambertian surface identically illuminated. This is the basic method of reflectance measurement for the bidirectional spectrometer in RELAB, and because the FTIR data are scaled to the bidirectional spectrometer data, this a reasonable form of the radiative transfer models of Hapke (1981, 1993) to investigate. The exact form of the multiple scattering equation is actually not critical as the objective here is to assess if these models can reproduce the systematics of the changes in the spectral features with particle size more than the exact reflectance values.

We therefore use Eq. (37) from Hapke (1981) and assume that the surface scatters light isotropically and that the viewing geometry is outside of the angular region of the strong backscattering lobe. The isotropic assumption is reasonable for nadir emergence angles and incidence angles  $<40^\circ$  (Mustard and Pieters 1989) and the standard viewing geometry for the bidirectional spectrometer ( $30^\circ$  incidence angle,  $0^\circ$  emergence) is well outside the angular width of the opposition surge. Reflectance is then calculated from 6 to 18  $\mu\text{m}$  for both olivine and quartz using the single-scattering albedo determined with Mie theory for each of the particle size distributions. These are plotted in Figs. 10 and 11 along with the measured reflectances of the particle size separates.

## RESULTS

### *Olivine*

The results for olivine (Fig. 10) show a high degree of agreement and thus Mie scattering explains many of the important first-order systematics observed in the reflectance spectra of fine olivine particulates. The positions of the absorption bands and reflectance peaks in the modeled reflectance spectra, however, do not match exactly with the measured reflectances. This may be due to the fact that the optical constants used are not those of the specific olivine sample for which the reflectance measurements were made.

*Volume scattering.* The model reflectances correctly predict most of the systematics observed in the volume scattering region. The reflectance of the finest particle size separate becomes the least of the separates well before the Christiansen feature. The reflectances of the successively larger size separates become less than the reflectance of the next largest size separate (or cross-over) at progressively longer wavelengths. The details are however different. In the measured reflectances, the 5–10- $\mu\text{m}$  separate exhibits a cross over near 6.2  $\mu\text{m}$  (Fig. 4), while in the modeled reflectances the cross-over is near 7.5  $\mu\text{m}$ . The 20–25- $\mu\text{m}$  separate has the lowest reflectance in the modeled spectra between 7 and 7.5  $\mu\text{m}$ , while it is intermediate in brightness in the actual reflectances. Nevertheless, the overall systematics in the modeled spectra are consistent with the measured data.

*Christiansen feature and restrahlen bands.* The modeled spectra correctly show the change in brightness in the Christiansen feature as a function of particle size and the broadening of the feature as particle size becomes small. This is specifically a consequence of the low scattering efficiency on either side of the feature, coupled with a non-negligible value for  $k$  in the middle of the feature. The modeled spectra also correctly show the relative reflectances of the restrahlen bands, with the larger particle sizes having higher reflectance than the smaller particle sizes. In addition, the modeled spectra show an evolution in the shape of the feature, with a decrease in spectra contrast and an increase in the slope toward longer wavelengths. Though the evolution of this feature is manifested slightly differently in the measured spectra, the basic trends are the same in that the decreases in reflectance are concentrated where  $k$  is large due to the increase in volume scattering. This imparts an overall increase in the spectral slope in the modeled spectra and a decrease in the negative spectral slope in the measured spectra. The differences in the details expressed are most likely due to differences between the actual values of  $n$  and  $k$  of the olivine and those used to calculate the spectra.

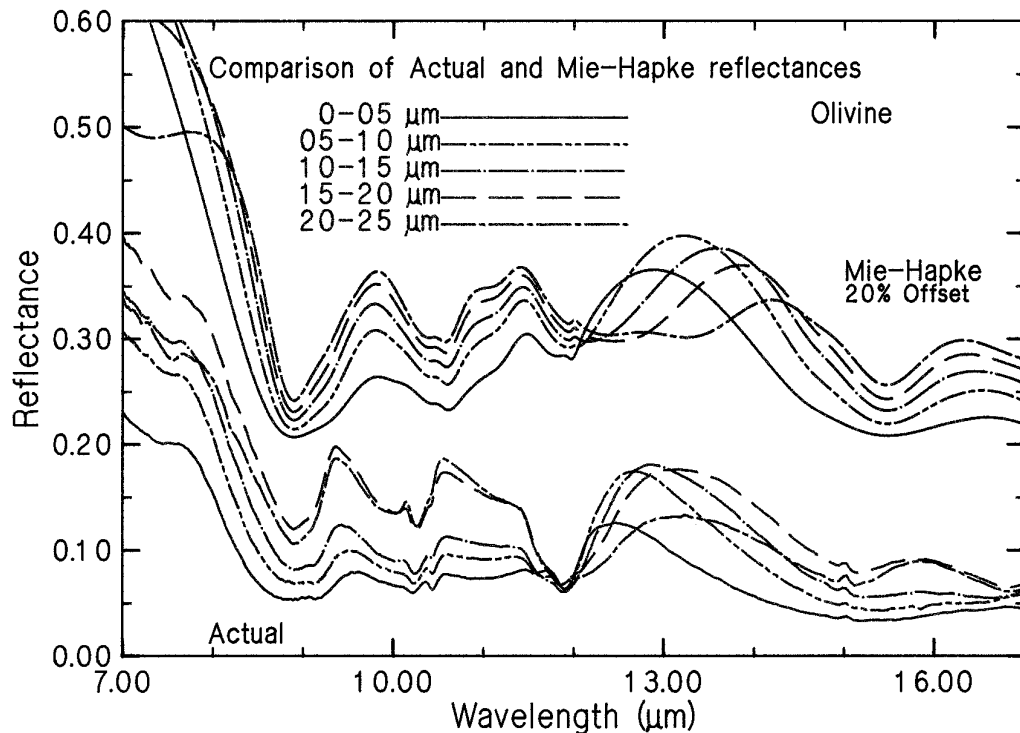


FIG. 10. Measured and theoretical Mie-Hapke reflectance spectra of the less than 25- $\mu\text{m}$  olivine size separates, from 7 to 17  $\mu\text{m}$ . The Mie-Hapke reflectances (offset by 0.2, or 20%, for clarity) are computed using the optical constants for olivine (Fig. 7) and a Mie model to determine single-scattering albedo followed by a Hapke model to determine reflectance. Note that the calculated spectra correctly reproduce the principal systematic changes observed in the measured spectra in the Christiansen feature ( $\approx 9 \mu\text{m}$ ), the restrahlen bands ( $\approx 9\text{--}11.5 \mu\text{m}$ ) and the transparency feature ( $\approx 12\text{--}15 \mu\text{m}$ ).

*Transparency feature.* The transparency feature in the modeled spectra shows exactly the same evolution as that observed in the measured spectra. The wavelength of the peak of the transparency features systematically shifts from longer to shorter wavelengths, and the intensity evolves from moderate values in the largest separate to the highest values in the 10–15- $\mu\text{m}$  separate and then drops in the 0–5- $\mu\text{m}$  separate. On the long wavelength side of the transparency feature,  $n$  approaches and becomes less than 1 near 15.4  $\mu\text{m}$  resulting in another Christiansen-type feature. The general systematics of this feature are also adequately simulated by the modeled spectra. The primary discrepancies between the modeled and actual spectra in the wavelength region of the transparency feature is that the modeled spectra show a greater contrast in wavelength position and spectral shape relative to the measured spectra. This may be due to a greater contribution from small particles than that accommodated by the particle size distributions used.

#### Quartz

The modeled spectra for quartz, shown in Fig. 11, exhibit good, first-order agreement with the measured spectra for

the transparency and Christiansen features, but exhibit significantly different behavior in the restrahlen bands.

*Volume scattering.* As discussed above, there is only one significant spectral cross-over observed in the quartz spectra; this occurs in the <5- $\mu\text{m}$  separate near 6.0  $\mu\text{m}$ . Though the modeled spectra predict a cross-over at a similar wavelength, they also predict cross-overs for the 5–10- and 10–15- $\mu\text{m}$  separates which are not observed. This is likely due to differences between the actual  $n$  and  $k$  for the quartz used in the measurements and those derived from the dispersion parameters of Spitzer and Kleinman (1961).

*Christiansen feature and restrahlen bands.* The Christiansen feature near 7.3  $\mu\text{m}$  is well modeled. In addition,  $n$  is near unity near 9.2 and 12.4  $\mu\text{m}$ , where Christiansen-type behavior is expected. However, since  $k$  is non-negligible in these wavelength regions, the spectra should exhibit a hybrid behavior. Indeed the modeled spectra exhibit minima near these wavelengths, although they are all near zero reflectance at 7.3  $\mu\text{m}$  while the measured spectra show a small increase in reflectance with the smallest particle size separates. The restrahlen bands between 7.3 and 9.5

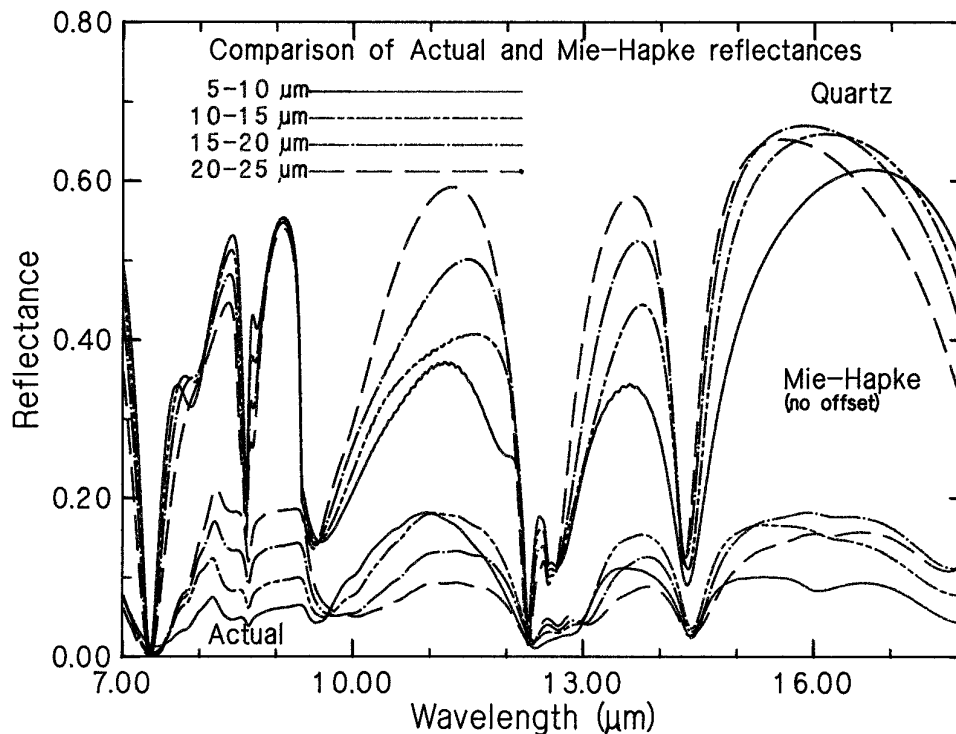


FIG. 11. Measured and theoretical Mie-Hapke reflectance spectra of the less than 25- $\mu\text{m}$  quartz size separates, from 7 to 17  $\mu\text{m}$ . The Mie-Hapke reflectances are computed using the optical constants for quartz (Fig. 7) and a Mie model to determine single-scattering albedo followed by a Hapke model to determine reflectance. The calculated spectra correctly reproduce some of the principal systematic changes observed in the measured spectra, primarily in the evolution of the transparency features ( $\approx 11$ , 13, and 16  $\mu\text{m}$ ). However, there are notable discrepancies in the restrahlen bands (7–9.5  $\mu\text{m}$ ) and in overall spectral contrast (the calculated spectra show much greater contrast).

$\mu\text{m}$  in the calculated spectra exhibit poor agreement with the measured spectra. While the measured spectra show an overall evolution of the bands with particle size, entirely consistent with the olivine measurements and calculations, the predicted spectra show none of the expected changes, except in the finest fractions. Here we see that the reflectances are somewhat lower and the band shape is slightly modified. In contrast, a region of anomalous dispersion is observed in 12.6  $\mu\text{m}$  which is similar to the restrahlen bands in behavior. Here the modeled spectra correctly predict the weakening of this feature with particle size.

The modeled spectra of Moersch and Christensen (1995) had similar problems in adequately matching the restrahlen bands. There are several possible reasons for this. The values of  $n$  and  $k$  may be in error, which was also suggested by Moersch and Christensen (1995) and more thoroughly demonstrated by Wald and Salisbury (1995). This is supported to some extent by the fact that there is good agreement between the modeled and measured spectra for olivine. Another possible explanation is that the Mie calculations are not valid for large values of  $n$  and  $k$ . The maximum values of  $n$  and  $k$  for olivine are a factor of 2–3 less than those for quartz, and the Mie calculations used

have not been verified for extreme values of  $n$  and  $k$  (Bohren and Huffman 1983). A third possibility is that the actual particle sizes are smaller or have very different particle shapes (e.g., platy) than the spherical assumed.

*Transparency feature.* There are three principal transparency features considered here which are located near 11.5, 13.5, and 16  $\mu\text{m}$ . The modeled spectra exhibit excellent first-order agreement with the measured spectra and are consistent with the qualitative analysis of  $D_c$  vs  $D_a$ . The modeled spectra correctly show the increase in reflectance with decreasing particle size, and the change in the symmetry of the band accompanied by a shift in the position of the wavelength of maximum reflectance. The amount of asymmetry produced and the wavelength shifts are consistent with the measured spectra. However, the measured spectra also exhibit a decrease in reflectance for the smallest size fractions, which is not predicted by the modeled spectra.

## SUMMARY AND CONCLUSIONS

Planetary surfaces consist primarily of particulate materials derived from bedrock through the processes of weath-

ering, alteration, and impacts. Remote sensing of the visible to mid-infrared reflected and emitted radiation from these surfaces provide essential compositional and material property information. However, because these remote sensing observations are necessarily dominated by scattering and absorption in these particulate mediums, it is important to understand in detail the effects of particle size on these measurements to quantitatively deconvolve the observations into information on composition and physical properties. Despite the progress in measuring and modeling observations for particulate materials where the typical particle size is greater than the wavelength of observation, there have been few systematic studies of the remote sensing properties of materials that have particle sizes comparable in size to the wavelength of observation. On many planetary surfaces, these particle size ranges may play a dominant role in remote sensing observations. For example, Pieters *et al.* (1993) show that the spectra of lunar soils is strongly affected by the  $<10\text{-}\mu\text{m}$  size fraction while the surface of Mars is dominated by dust with a typical particle size estimated to be  $\leq 5\text{ }\mu\text{m}$  (Pollack *et al.* 1979, Christensen and Moore 1992).

In this study, we have made systematic observations of reflectance spectra from 0.3 to 25  $\mu\text{m}$  of particles that are comparable to the wavelength. Using the minerals olivine and quartz, and 5- $\mu\text{m}$  size separates between 0 and 25  $\mu\text{m}$ , a number of distinct changes in the reflectance properties were observed as a function of decreasing particle size. (1) In the region of volume scattering ( $n$  is moderate,  $k \ll 1.0$ ), when the particle size is comparable to the wavelength of the radiation, a sharp drop in reflectance is observed. (2) In the wavelength region of the restrahlen bands ( $k > 0.1$ ), the reflectance spectra show a continuous decrease in reflectance with particle size, and there are no distinct or anomalous effects observed when the particle size and wavelength of light are comparable. However, the shape of the restrahlen bands evolve systematically with particle size. (3) When  $k$  is non-negligible, the Christiansen feature is observed to saturate and broaden to both the short and long wavelengths sides of the feature (e.g., olivine). When  $k$  is very small, this band is relatively invariant with particle size (e.g., quartz). (4) The transparency features are observed to exhibit several systematic changes with these small particle size separates. In general, the feature shows an increase, and then a decrease in spectral contrast, the wavelength position of the reflectance maximum typically shifts to shorter wavelengths, and the features show a change in symmetry.

These general systematics can be understood qualitatively through the application of the general properties of Mie scattering for particles that are comparable to the wavelength of light. The theory predicts that when the particle size decreases to become comparable to the wavelength of light when  $k$  is small and  $n$  is moderate, then the

extinction exhibits a rapid decline. The principle reason for this is that when the particle is small relative to the wavelength, the particle as a whole interacts with the electromagnetic radiation, and the processes of this interaction can no longer be broken down into the surface and volume scattering components principally because of diffraction. The decline in scattering efficiency is proportional to  $1/(\lambda^4)$  while the decline in absorption efficiency is proportional to  $1/(\lambda)$ . Therefore, as extinction efficiency declines, the absorption efficiency does not decline as rapidly as the scattering efficiency. Thus the single-scattering albedo, and hence reflectance, exhibits a sharp decline, as was observed in the principal regions of volume scattering in the reflectance spectra. This property of the Mie solution can be used with the optical constants to define a critical diameter ( $D_c$ , valid when  $k$  is small) as a function of wavelength for which a sharp decline in reflectance is expected. This concept of the critical diameter ( $D_c$ ) was shown to be a useful tool to understanding the systematic changes in the reflectance properties with particle size.

The ultimate goal for remote sensing of planetary surfaces is to extract quantitative information on the physical and compositional properties. We therefore modeled the reflectance spectra of the fine particle separates using a combination of Mie theory to determine the single-scattering albedo and a Hapke model to calculate the reflectance. The results for olivine showed, in general, a good correspondence between the measured and modeled reflectance spectra. The spectral contrast of the modeled spectra were very similar to the measured spectra, and, more importantly, the modeled spectra correctly showed the broadening of the Christiansen feature, the progressive weakening of the restrahlen bands, and the systematic changes in the transparency feature with decreasing particle size. Differences between the measured and modeled spectra are likely due to the fact that the optical constants used were not measured of the specific sample measured in the laboratory. In contrast, the results for the modeling of the quartz spectra were mixed. Though the computed spectra correctly modeled the basic evolution of the transparency features with particle size (change in contrast, wavelength position of the reflectance maximum, symmetry), and the relative invariance of the Christiansen feature, the overall spectral contrast of the modeled spectra were a factor of 2–3 higher than the measured spectra, and the overall behavior of the restrahlen bands were significantly different from the measured spectra.

There are several possible reasons for these discrepancies. It is apparent that models of fine particle spectral properties must explicitly incorporate Mie-type behavior. Moersch and Christensen (1995) showed that models dependent solely on geometric optics were inadequate and the incorporation of Mie theory in multiple scattering models provided the best fit in their measurements of quartz

emission spectra as a function of particle size. Our results support this conclusion. However, the methods to incorporate a Mie scattering solution into a multiple scattering model need to be thoroughly investigated. We simply used the Mie results for extinction and scattering efficiency to calculate single-scattering albedo. This ignores the fact that the Mie solution explicitly includes diffraction and assumes that the particles are separated by at least 3 particle radii. This is clearly not the case in soils where the particles are in physical contact. The importance of diffraction and the correct methodology to include these effects is not well defined at this time. Also, the extinction efficiency for the Mie solutions is  $\approx 2$  for particles larger than the wavelength while it is assumed to be 1 for particulate surfaces (Hapke 1993). Wald (1994) derived a simple correction for using Mie scattering for close-packed particles, termed diffraction subtraction, where the corrected single-scattering albedo is twice the Mie single-scattering albedo minus 1. This correction was used in the calculations of Moersch and Christensen (1995) for their Mie–Hapke hybrid models. However, this is not rigorously defined and causes negative albedos for single-scattering albedos less than 0.5. A more realistic treatment of diffraction in particulate soils is necessary. Another reason for the discrepancies is that validity of the models for large values of  $n$  and  $k$  is not well understood. Most of the development and testing of the models has been for values of  $n$  and  $k$  much less than those exhibited by quartz in the reststrahlen bands. Finally, the specific values of  $n$  and  $k$  are critical to the calculations, especially for the transitions between strong and weak absorptions. As noted by Moersch and Christensen (1995), there may be problems with the published values of  $n$  and  $k$  for quartz derived by Spitzer and Kleinman (1961).

### ACKNOWLEDGMENTS

The authors warmly acknowledge the contributions to this work from J. Salisbury and P. Christensen who acquired DHR and emission spectra of the olivine samples and for their helpful discussions of the work while in progress. We also thank S. Clemens for his generous assistance in acquiring data on the particle size distributions. Formal reviews by J. Salisbury, J. Moersch, as well as thoughtful discussions with C. Pieters, M. Weinrich, B. Hapke, R. Clark, and S. Pratt have all contributed substantially to this work, though any errors or omissions are our responsibility. This work is supported by the NASA Planetary Geology and Geophysics Program under Grant NAGW-3379.

### REFERENCES

- ARONSON, J. R., AND A. G. EMSLIE 1973. Spectral reflectance and emittance of particulate materials. 2. Applications and Results. *Appl. Opt.* **12**, 2573–2584.
- BOHREN, C. F., AND D. R. HUFFMAN 1983. *Absorption and Scattering of Light by Small Particles*. Wiley, New York.
- CARRIER, W. D., G. R. OLHOEFT, AND W. MENDELL 1991. Physical properties of the lunar surface. In *Lunar Sourcebook. A User's Guide to the Moon* (G. H. Heiken, D. T. Vaniman, and B. M. French, Eds.), pp. 475–567. Cambridge Univ. Press, Cambridge.
- CHRISTENSEN, P. R., *et al.* 1992. Thermal emission spectrometer experiment: Mars observer mission. *J. Geophys. Res.* **97**, 7719–7735.
- CHRISTENSEN, P. R., AND H. J. MOORE 1992. The martian surface layer. In *Mars* (H. H. Kieffer, B. M. Jakosky, C. W. Snyder, and M. S. Matthews, Eds.), pp. 686–729. Univ. of Arizona Press, Tucson.
- CHRISTENSEN, P. R., AND S. T. HARRISON 1993. Thermal infrared emission spectroscopy of natural surfaces: Application to desert varnish coatings on rocks. *J. Geophys. Res.* **98**, 19,819–19,834.
- CONEL, J. E. 1969. Infrared emissivities of silicates: Experimental results and a cloudy atmosphere model of spectral emission from condensed particulate mediums. *J. Geophys. Res.* **74**, 1614–1634.
- CROWN, D. A., AND C. M. PIETERS 1987. Spectral properties of plagioclase and pyroxene mixtures and the interpretation of lunar soil spectra. *Icarus* **72**, 492–506.
- GAFFEY, S. J., L. A. MCFADDEN, D. NASH, AND C. M. PIETERS 1993. Ultraviolet, visible, and near-infrared reflectance spectroscopy: Laboratory spectra of geologic materials. In *Remote Geochemical Analysis: Elemental and Mineralogical Composition* (C. M. Pieters and P. J. Englert, Eds.), pp. 43–78. Cambridge Univ. Press, Cambridge.
- HAPKE, B. 1981. Bidirectional reflectance spectroscopy, 1. Theory. *J. Geophys. Res.* **86**, 3039–3054.
- HAPKE, B. 1993. *Theory of Reflectance and Emittance Spectroscopy*. Cambridge Univ. Press, Cambridge.
- HAPKE, B. 1996. A model of radiative and conductive energy transfer in planetary regoliths. *J. Geophys. Res.*, in press.
- HIROI, T., AND C. M. PIETERS 1994. Estimation of grain sizes and mixing ratios of fine powder mixtures of common geologic mineral. *J. Geophys. Res.* **99**, 10,867–10,879.
- HUNT, G. R., AND R. K. VINCENT 1968. The behavior of spectral features in the infrared emission from particulate surfaces of various grain sizes. *J. Geophys. Res.* **73**, 6039–6046.
- LYON, R. J. P. 1964. *Evaluation of Infrared Spectrophotometry for Compositional Analysis of Lunar and Planetary Soils, Part II, Rough and Powdered Surfaces*. NASA Report CR-100.
- LYON, R. J. P. 1965. Analysis of rocks by spectral infrared emission (8 to 25 Microns). *Econ. Geol.* **60**, 717–736.
- MOERSCH, J. E., AND P. R. CHRISTENSEN 1995. Thermal emission from particulate surfaces: A comparison of scattering models with measured spectra. *J. Geophys. Res.* **100**, 7465–7477.
- MUKAI, T., AND C. KOIKE 1990. Optical constants of olivine particles between wavelengths of 7 and 200  $\mu\text{m}$ . *Icarus* **87**, 180–187.
- MUSTARD, J. F., AND C. M. PIETERS 1989. Photometric phase functions of common geologic minerals and applications to quantitative analysis of mineral mixture reflectance spectra. *J. Geophys. Res.* **94**, 13,619–13,634.
- PIETERS, C. M. 1983. Strength of mineral absorption features in the transmitted component of near-infrared reflected light: First results from RELAB. *J. Geophys. Res.* **88**, 9534–9544.
- PIETERS, C. M., E. M. FISCHER, O. RODE, AND A. BASU 1993. Optical effects of space weathering: The role of the finest fraction. *J. Geophys. Res.* **98**, 20,817–20,824.
- POLLACK, J. B., D. S. COLBURN, F. M. FLASER, R. KAHN, C. E. CARLSTON, AND D. C. PIDEK 1979. Properties and effects of dust particles suspended in the martian atmosphere. *J. Geophys. Res.* **84**, 2929–2945.
- SALISBURY, J. W. 1993. Mid-infrared spectroscopy: Laboratory data. In *Remote Geochemical Analysis: Elemental and Mineralogical Composition* (C. M. Pieters and P. A. Englert, Eds.), pp. 79–98. Cambridge Univ. Press, Cambridge.

- SALISBURY, J. W., AND A. WALD 1992. The role of volume scattering in reducing spectral contrast in spectra of powdered minerals. *Icarus* **96**, 121–128.
- SALISBURY, J. W., L. S. WALTER, N. VERGO, AND D. M. D'ARIA 1992. *Infrared (2.1–25  $\mu\text{m}$ ) Spectra of Minerals*. Johns Hopkins Univ. Press, Baltimore, MD.
- SALISBURY, J. W., AND L. S. WALTER 1989. Thermal infrared (2.5 to 13.5  $\mu\text{m}$ ) spectroscopic remote sensing of igneous rock types on particulate planetary surfaces. *J. Geophys. Res.* **94**, 9192–9202.
- SPITZER, W. G., AND D. A. KLEINMAN 1960. Infrared lattice bands of quartz. *Phys. Rev.* **121**, 1324–1335.
- VINCENT, R. K., AND G. R. HUNT 1968. Infrared reflectance from mat surfaces. *Appl. Opt.* **7**, 53–58.
- WALD, A. E. 1992. Modeling thermal infrared (2–14  $\mu\text{m}$ ) reflectance spectra of frost and snow. *J. Geophys. Res.* **99**, 24,241–24,250.
- WALD, A. E., AND J. W. SALISBURY 1995. Thermal infrared directional emissivity of powdered quartz. *J. Geophys. Res.* **100**, 24,665–24,675.